EXPERIMENTAL STUDY AND NUMERICAL SIMULATION OF FLOW AROUND WING CONTROL SURFACE

G. Fillola, Airbus

G. Carrier, J-B. Dor, ONERA

Keywords: *Spoiler and aileron, CFD, Unsteady transonic flow, HTP and VTP*

Abstract

This paper examines the capability of CFD methods based on RANS equations to simulate spoiler and aileron setting effects and evaluates its accuracy by comparison to wind tunnel tests. Thus, a specific wind tunnel (w/t) test campaign has been conducted in ONERA T2 facility to determine effects of spoiler and aileron setting on a basic extruded profile. Following are numerical simulations of these tests, including not only the profile but also the w/t walls.
Finally, the end of the paper focuses on industrial applications of CFD performed at Airbus. Particularly, the interaction between spoiler and horizontal/vertical tail planes are pointed out.

INTRODUCTION

The correct prediction of handling qualities and hinge moments induced by the deployment of wing control surfaces (e.g. spoilers and ailerons) is a crucial point in the general aircraft sizing process with a major impact on the final aircraft weight. Traditionally, only very time consuming and costly wind tunnel tests, and semi-empirical methods were used to elaborate these data. Therefore, CFD appears as an attractive compromise between cost and accuracy to improve and complete this process.

Thus, in order to enrich the aero-modeling engineer "toolbox", AIRBUS and ONERA took part in a French national project, namely *DTP Modeling*. One task of this project was dedicated to the development/validation of predictive computational methods for the evaluation of wing control devices effectiveness. In this framework, w/t testing has been conducted for an extruded profile equipped with both an aileron and a spoiler. The objective of these tests were twofold: first, to obtain a better understanding of the major flow phenomena involved in control surfaces deflection, second, to provide a wide database for CFD validation.

This paper describes the experimental tests and the associated numerical validations. Some industrial applications of CFD performed at Airbus are then presented at the end.

1 2D NUMERICAL & EXPERIMENTAL ANALYSIS

1-1 Experimental setup

The model is a transonic profile OAT15A, having a maximum thickness of 12.5%-chord and a trailing edge thickness of 0.5%-chord. It is equipped with deflectable aileron and spoiler (see fig. 1) that can be adjusted to operate several settings. The hinge-line for the aileron is located at 80%-chord and the spoiler one at 60%-chord.

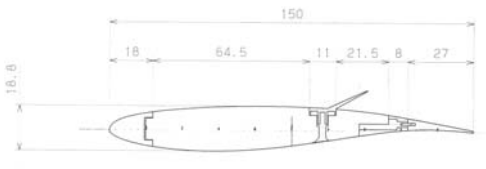

fig. 1 : Test mockup

The tests were conducted in the ONERA-T2 facility of ONERA-DMAE (see fig. 2). T2 is an air-injected closed-circuit wind tunnel (w/t). The upper and lower walls shapes are automatically adjusted to minimize the influence of the w/t wall on the flow around the profile (see [1]).

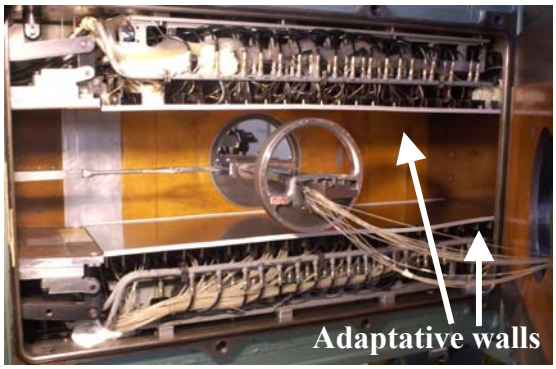

fig. 2 : ONERA-T2 w/t facility

The mock-up is equipped with both steady and unsteady pressure probes. 80 steady pressure probes are equitabily positioned all along of the middle chord. 12 Kulite probes are situated on the upper side of profile below the spoiler and one is placed on the lower side at 50% of the chord.

Transition is fixed at 7% of the chord with a rough carborundum band on both upper and lower side. Aerodynamic characteristics available from this test program are in the form of lift and pitching moment derived from integration of model centerline pressure distribution. Drag is evaluated by downstream wake survey measurements.

Additional measurements using LDV (Laser Doppler Velocimetry) and oil flow visualizations were also conducted in order to investigate some detail of the flow and to measure the boundary layer quantities.

1-2 Major experimental results

Global coefficients on profile with deflected aileron are represented on fig. 3. Results are in good agreement with aerodynamic theory: lift increases as aileron is trailing-edge-down deflected. For low Cz (~0.6), drag is not really affected by aileron deflection. Moreover, α_{max} decreases with trailing-edge-down deflection; that is quite consistent with linear theory, which formulates a linear behaviour of the angle of attack of adaptation with angle of deflection.

$$\alpha = -K\delta_p \qquad (1)$$

where K depends on aileron hinge-line position

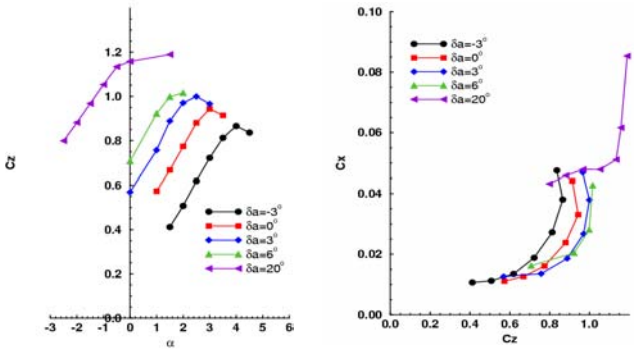

fig. 3 : global coefficient on profile with aileron deflected, M=0.73 Rec=3.2.10^6

Pressure distributions on the profile with several deflected aileron are depicted in fig. 4. For low deflection angle (-3° and 3°), aileron trailing-edge-down setting leads to an aft movement of the shock, whereas at high deflection angle (+6° and 20°), the separation area appearing on aileron upper surface prevents then shock to move backward.

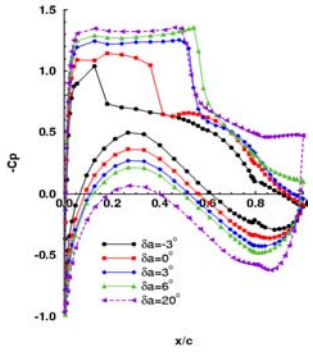

fig. 4 : pressure distribution on the profile with aileron deflected, M=0.73, Rec=3.2.10^6

Global coefficients on profile with deployed spoiler are represented in fig. 5. The spoiler setting leads to a reduction of lift and a drag increase, but this behaviour is not exactly proportional to setting angle.

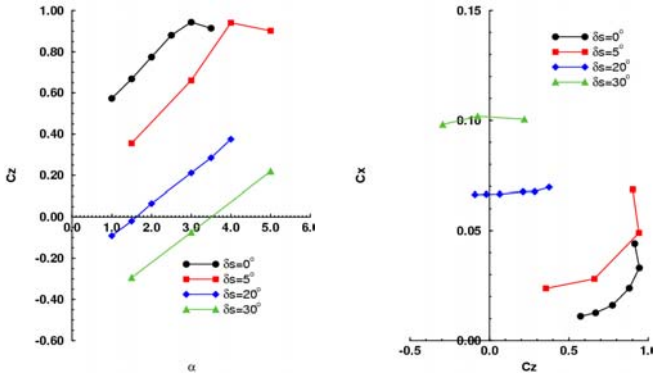

fig. 5 : global coefficient on profile with aileron deflected, M=0.73 Rec=3.2.10^6

LDV measurements give an overview of the flow patterns behind the spoiler (see fig. 6). A large separation area appears that leads to pressure plateau on profile pressure distribution (fig. 7) and results in the drag increase. The spoiler setting causes the downwash to decrease and the circulation around the profile is therefore deeply modified. Thus, the upper profile leading edge suction peak decreases whereas the lower profile one increases, causing the lift to decrease. An interesting feature is the analysis of frequential spectrum of unsteady pressure probes (fig. 7). Each probe shows an amplified frequency of about 3000 Hz. As suggested by Bodapati [3] and McLachlan [10], we built a Strouhal number with l_{ref} the distance between spoiler and airfoil trailing edges and U_{ref} the upstream velocity. That leads to a value of 0.1, which is representative of a vortex shedding. (This Strouhal number is constant for each spoiler deflection and each Mach number, justifying the choice of the reference length)

$$St = \frac{f \times l_{ref}}{U_{ref}} \qquad (2)$$

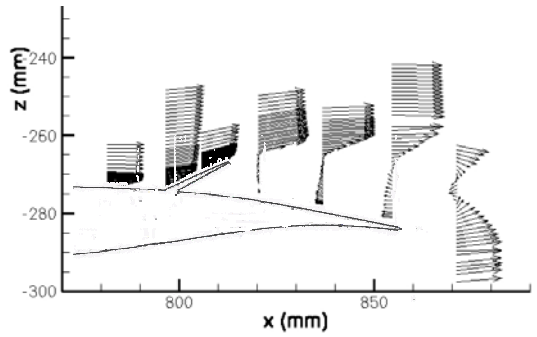

fig. 6 : Flow pattern after the spoiler depicted by LDV measurements

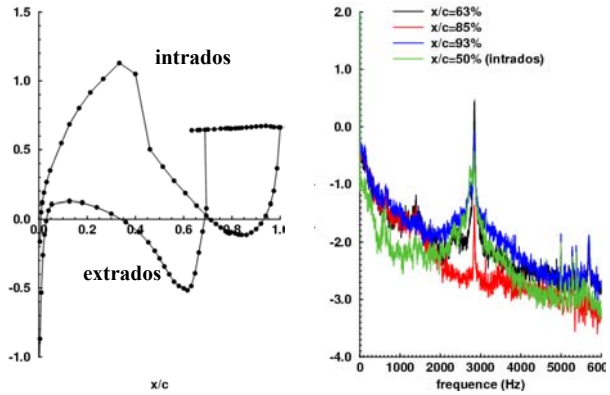

fig. 7 : Steady pressure distribution and frequential spectrum on spoiler deflected profile, M=0.73, α=3°, Rec=3.2.10^6

1-3 Numerical method in elsA solver

The numerical analysis has been carried out with ***elsA*** solver. It has been designed by ONERA, CERFACS and AIRBUS, according to an Object Oriented design method and it is mainly coded with C++ language, even though the most CPU-expensive loops are coded with FORTRAN language for better numerical efficiency (see [9]).

The main features and numerical functions of ***elsA*** solver are listed below:

- Cell centered code dealing with structured meshes.
- Classical central scheme for Euler model (centered flux with scalar dissipation)
- Viscous flux computed from cell-centered evaluations of velocity and temperature gradients, with possible correction values at interfaces.
- Classical algebraic and transport equations turbulence models (all of them following Boussinesq's assumption).
- Backward-Euler time integration associated with the LU implicit method.
- Wall Law treatment possibility for wall boundary condition.

1-4 Numerical and meshing strategy

Previous numerical studies of T2 W/T have shown that, for transonic conditions, despite of the adaptation of T2 upper and lower wall, the flow at the center of the tunnel is not completely bi-dimensional (see [2]). This is mainly due to the remaining interaction between the shock and the lateral tunnel walls. Works of Jiang [8] and Garbaruk, Shur & Strelets [6] also suggest that the good assessment of bi-dimensional profile characteristics requires the complete modeling of the W/T

It was therefore chosen to simulate the complete w/t geometry, including OAT15A profile, upper, lower and lateral T2 walls. Meshes topology are shown in fig. 8. As suggested by Bezard in [4], these meshes have been extended of about 500 mm upstream in order to assess the good boundary layer thickness in w/t entrance. Actually, the mesh on

clean airfoil has 1.6M nodes and mesh around profile with spoiler 2.2M.

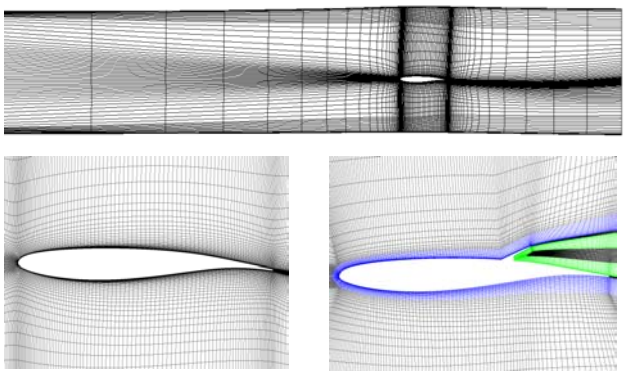

fig. 8 : top: OAT15A + T2 w/t wall mesh, left: clean profile or aileron profile topology, right: spoiler topology

In order to improve the meshing process, a mesh deformation procedure has been used (it is described in [5]). Thus, rotation of the profile, w/t wall adaptation and aileron deflection can be taken into account without re-meshing phase (shown in fig. 9)

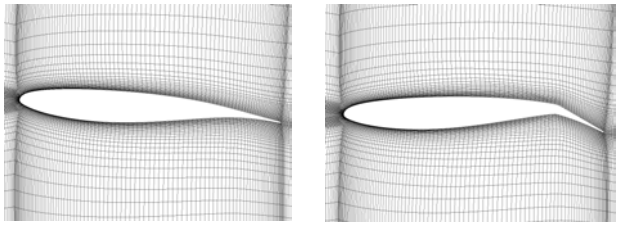

fig. 9 : Mesh deformation procedure, left : clean airfoil at α=5°, right : airfoil with 20° deflected aileron at α=0°

The following boundary conditions have been applied to our calculation in order to assess a good representatitivity of the physical problem:

- *w/t entrance section*: injection condition (α, β, Pi, Ti fixed)
- *w/t exit section* : pressure imposed condition (that must be adjusted in order to impose the upstream Mach number)
- *w/t wall and airfoil skin* : adiabatic wall condition

1-5 CFD vs. Experimental results

In this section, we compare CFD results to w/t tests and we try to explain discrepancies and agreement between both.

1-5.1 Clean profile and deflected aileron

Simulations have been performed on clean airfoil and three deflected aileron configurations: δp=-3°, 3°, 6°

The two most common turbulence models used in Airbus have been tested: Spalart-Allmaras model [SA] and Kok k-ω model [Kok]. For transonic condition, [SA] does not allow converging a solution. This is mainly due to the interaction shock/boundary layer at the intersection between profile and lateral wall: A coupling between the shock and separation area prevents from establishing a steady solution.

[Kok] model allows obtaining a steady solution, but for each configuration a too aft shock position is found compared to w/t tests (see fig. 10). Moreover, one can see that separation occurring at airfoil trailing edge for δp=3° and 6° is clearly under-estimated by CFD. The fig. 11 plots a comparison between velocity profile near airfoil skin measured by LDV and the computed ones: at station x/c=96% (trailing edge), it is clear that the separation area predicted by tests is not well captured by CFD.

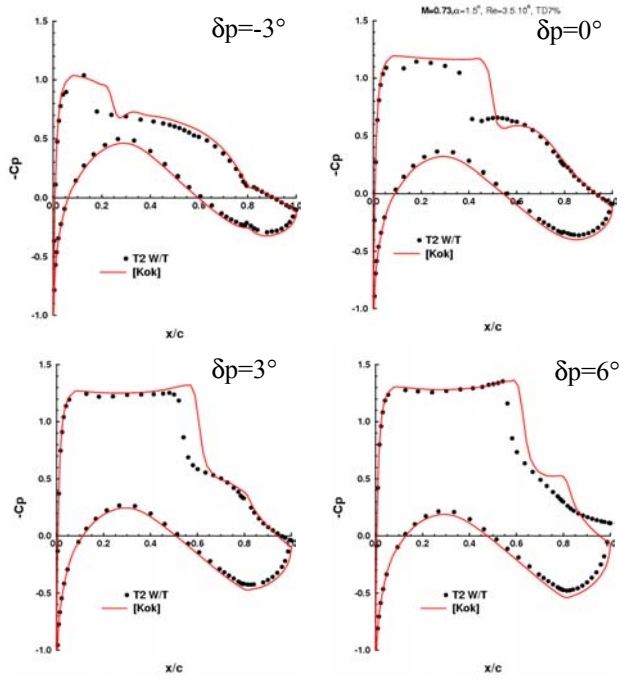

fig. 10 : Pressure distribution around airfoil with aileron deflected, M=0.73, α=1.5° Rec=3.2.10^6

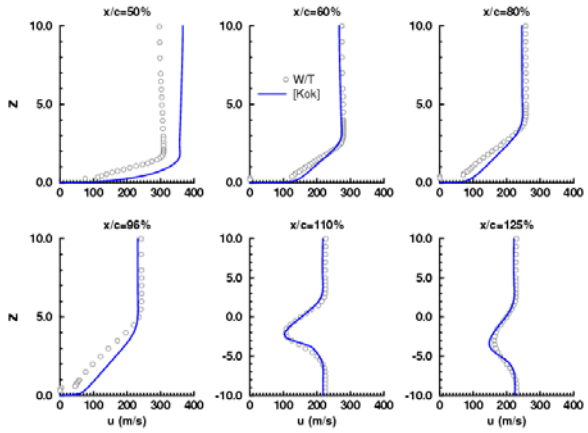

fig. 11 : Velocity profile around airfoil with 3° aileron deflected, M=0.73, α=1.5° Rec=3.2.10^6

Therefore, the global coefficient Cz and Cx are over-estimated for each configuration. Nevertheless, having a look on aileron effectiveness (fig. 12), one can notice that the agreement between CFD and experiment is quite good. Conclusion is then: even if CFD is not able to accurately predict the characteristics of the clean airfoil of these experiment, the pure aileron effect is well captured.

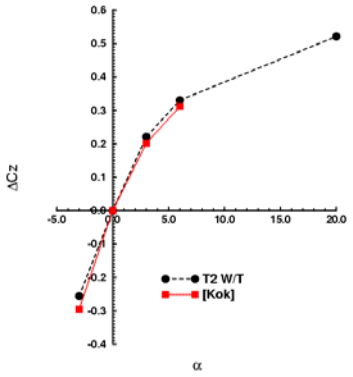

fig. 12 : Aileron effectiveness, M=0.73, α=1.5° Rec=3.2.10^6

1-5.2 Profile with deployed spoiler

Computations have been performed on the profile with spoiler configurations: δsp=20°, 30°

[SA] et [Kok] model have been tested. A steady solution has been obtained with [SA] whereas [Kok] converges on an erratic way and seems to calculate an unsteady periodic solution. The visualization of the wake via turbulent viscosity confirms this (see fig. 13).

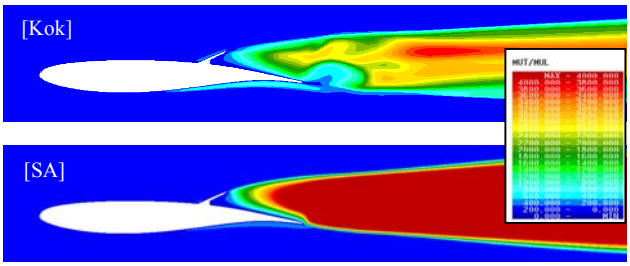

fig. 13 : μ_t/μ field after the spoiler, top : [Kok] model, back : [SA] model

Steady analysis

The agreement between steady solution calculated with [SA] model and experiment is quite good (fig. 14) for both angles of deflection. Except in the area behind the spoiler where the pressure plateau is overestimated. Anyway, the computed global coefficients are quite similar to experimental ones (see fig. 15); some remaining discrepancies on total drag are surely due the estimation of viscous pressure drag behind the spoiler.

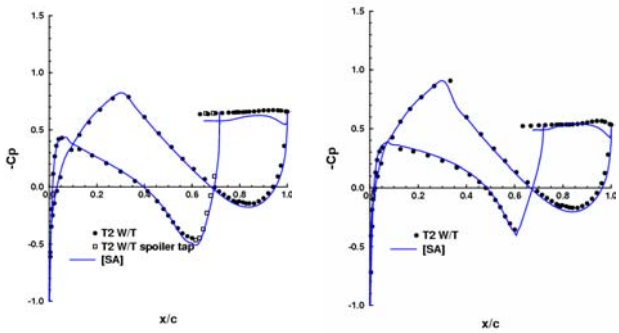

fig. 14 : Pressure distribution on the profile, M=0.73, α=3°, left : δsp=30°, right : δsp=20° Rec=3.2.10^6

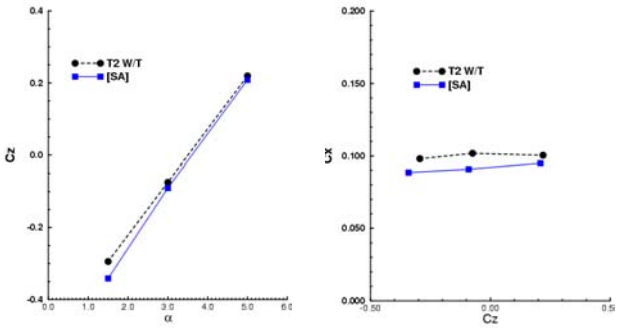

fig. 15 : Lift and drag polars, δsp=30°, M=0.85 Rec=3.2.10^6

Unsteady analysis

Unsteady computations have been carried out with [Kok] model. In order to cope with CPU and memory cost, we only use a 2D mesh (C mesh of 84.000 nodes). Several Mach number, setting angle and angles of attack were investigated.

For unsteady calculations, the dual time stepping (DTS) approach is used: In order to target frequencies between 1000Hz and 4000Hz, we chose a global time step equal to 8.10^{-6} second, which allows having 30 to 125 iterations per period according to initial conditions.

Periodic unsteady convergence has been achieved with the following strategy:

- 500 steady cycles (Local time stepping)
- 3000 unsteady cycles with DTS

Convergence of Cz coefficient is plotted on fig. 16.

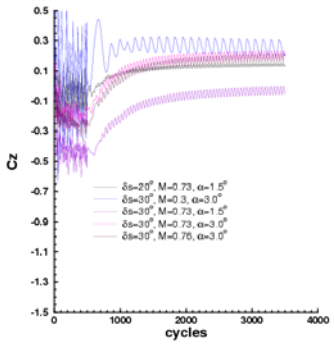

fig. 16 : Convergence history of unsteady calculations

The table 1 sums up the results of this calculation. First, the frequency of the phenomena is well captured by CFD for all Mach numbers, all angles of attack and all spoiler deflections. Thus, a constant Strouhal number of 0.1 (as defined by formula (2)) can be found, that is quite consistent with the experiment. This periodic phenomenon can be visualized via vorticity post-processing (see fig. 17): two vortices alternatively formed at spoiler trailing edge and airfoil trailing edge. This instability is well known as Kelvin-Helmoltz one. It is a non-viscous instability that is due to fluid inertia: the mixing layer between convective flow and separation area behind spoiler is highly rotational and then induces vortex shedding.

Nevertheless, the average lift given by the calculation is not in accordance with the one given by the steady pressure probe of the experimental mock-up. For example, at M=0.73 and α=3°, experiment give Cz=-0.1 whereas calculation Cz=0.21. Moreover, fig. 18 compares 2D unsteady numerical pressure distribution at maximum and minimum lift at averaged experimental pressure distribution: it appears that numerical calculations oscillate around a different averaged state than experimental one.

δsp	Mach	α(°)	Cz_{moy}	Cz_{RMS}	Strouhal
20°	0.73	3	0.43	0.03	0.1
30°	0.3	3	0.26	0.05	0.1
	0.73	1.5	-0. 03	0.03	0.1
		3	0.21	0.02	0.1
	0.76	3	3	0.03	0.1

table 1 : Unsteady calculation resume

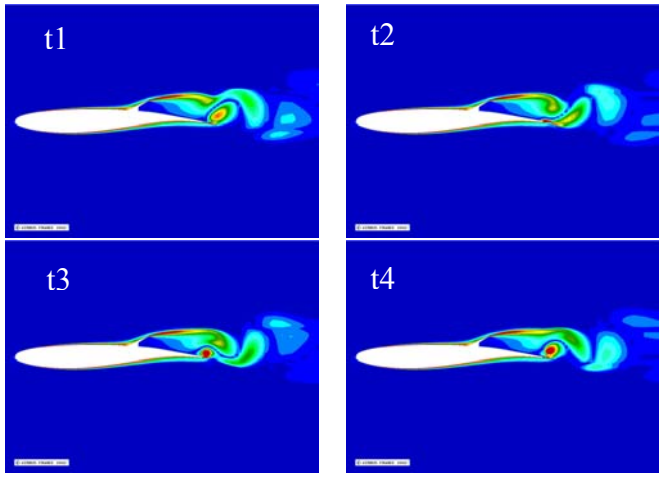

fig. 17 : Vorticity field δsp=30°, M=0.73, α=3°, Vortex shedding

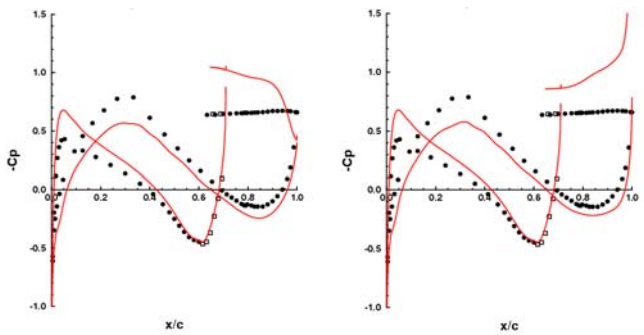

fig. 18 : Pressure distribution at minimum lift and maximum lift, M=0.73, α=3°, δsp=30°, Rec=$3.2.10^6$

2 INDUSTRIAL APPLICATIONS

This section is dedicated to the description of industrial use of CFD in Airbus to generate aerodynamic data for handling qualities. It follows up the results presented in [5] concerning the simulation of spoiler deflection on a wing/body without tails and complete them by the simulation of horizontal and vertical tail planes.

2-1 Reminder: spoiler setting simulation

The spoiler deflection is simulated via an ***Overset Chimera*** approach (see [11] and [7]) in order to ease the meshing process: one domain is dedicated to the wing body (with the classical topology used in Airbus) whereas another one, independent from the previous one, is dedicated to the spoiler (see fig. 19).

To validate our calculations, we rely on experimental results coming from a wind tunnel test campaign with mainly balance measurements. The mock-up is a complete aircraft with nacelles, flap-track-fairings, horizontal and vertical tail planes (H/VTP), and is compared to calculations around a simple wing-body. The wing shape corresponds to wind tunnel condition (5.10^6 Reynolds number) and is assumed as rigid when spoilers are deflected.

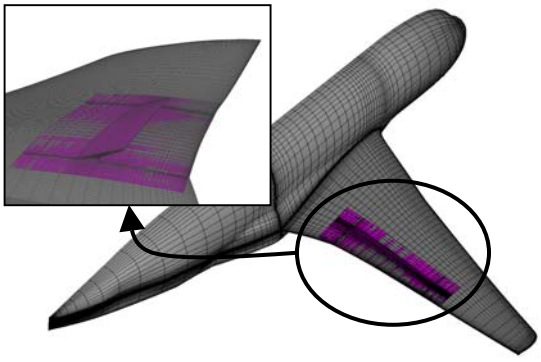

fig. 19 : Airbus aircraft with 20° deflected spoiler

Lift and drag effectiveness are represented on fig. 20. A good agreement between experiment and numerical calculations is found, as much on the linear part of the curve as on the non-linearity.

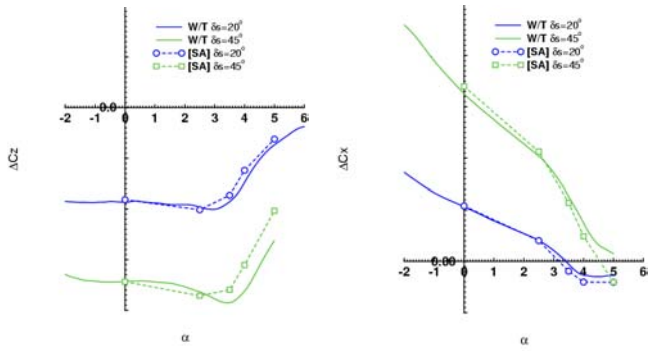

fig. 20 : Lift and drag effectiveness, δsp=20°, M=0.85

To assess the rolling moment, we demonstrated the necessity to simulate the dissymmetrical aircraft. This is due to an interaction between right and left wing.

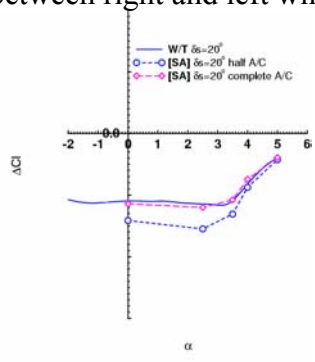

fig. 21 : Rolling moment, δsp=20° (left wing), M=0.85

2-2 Horizontal and vertical tail plan effect

Tails are also simulated with the Chimera meshing approach, by adding two independent domains to the previous wing/body/spoiler mesh.

On the basis of the several elementary meshes, three complex meshes can be assembled as to define several a/c configurations:

1. Clean wing with tails (half a/c, 5.5M nodes)
2. Wing/spoiler/tails, airbrake (half a/c, 6M nodes)
3. Wing/spoiler/tails, spoiler (Complete a/c, 12.5 nodes, see fig. 22)

The impact of each device can be thus isolated and so identified.

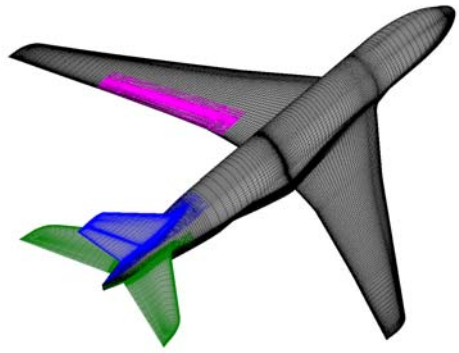

fig. 22 : AIRCRAFT with 20° deflected spoiler, HTP and VTP

Clean wing with tails

We will start by analyzing the impact of tails on the clean wing. The fig. 23 compares the pitching moment of the configuration with and without tail. The effect of HTP is well captured by CFD; indeed, both CFD and experiment see an increase of Cm_α slope of 109% by the HTP.

The experimental slope is not exactly equal to the numerical one, because nacelle has not been modeled by CFD. Their impact has been experimentally measured and can be assimilated to an aft movement of the aerodynamic center of about 6.5% of amc. The application of this correction on the numerical results allows correcting the Cm_α slope in a good manner.

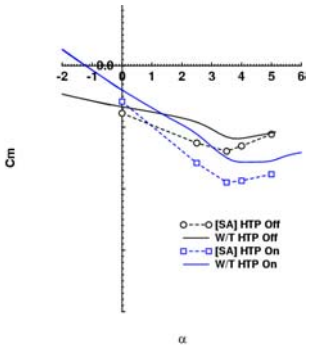

fig. 23 : Pitching moment of configuration with or without HTP, clean wing, M=0.85

Wing/body with spoiler and tails, Airbrakes

In this paragraph, the impact of HTP on spoiler effectiveness is analyzed. The fig. 24 shows the pitching moment effectiveness of the configurations with and without tails. The modeling of HTP allows having a good agreement between CFD and experiments.

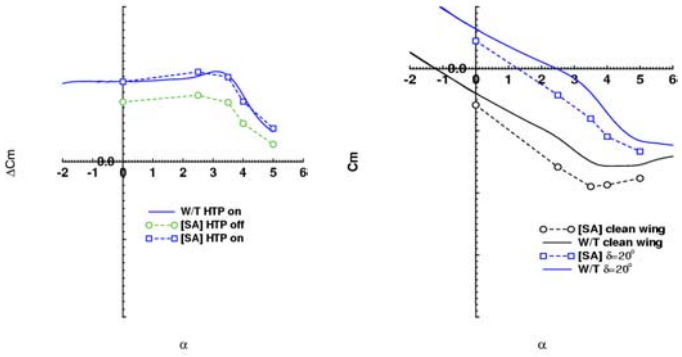

fig. 24 : Pitching moment effectiveness, δsp=20°, M=0.85

Moreover, the discrepancy between the HTP off/ HTP on effectiveness highlights an interaction between spoiler and HTP, that can be explained by two phenomena. First, the spoiler deployment modifies the downwash of the flow behind the spoiler (§1-2), that is seen by the HTP as a decrease of its effective angle of attack. Second, the internal spoiler tip vortex meets HTP tip (see fig. 25): total pressure loss, associated to a reduction of local angle of attack due to induced velocity vy created by the vortex, limits the HTP lower side over-speed on external section (see fig. 26).

Finally, both phenomena induce a pitch up moment of the A/C.

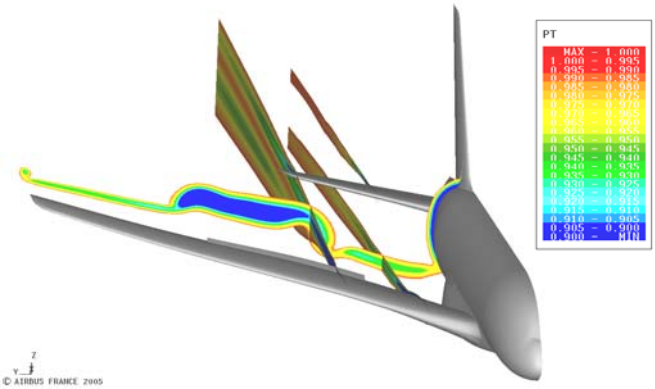

fig. 25 : total pressure field after the spoiler, δsp=20°, α=2.5°, M=0.85

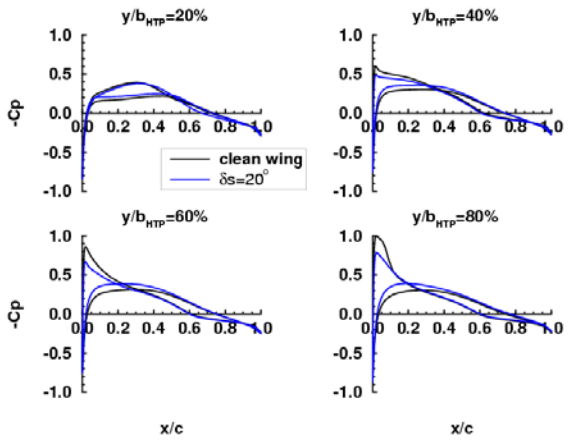

fig. 26 : Pressure distribution on HTP, M=0.85, α=2.5°

Wing/body with spoiler and tails, Spoiler

The impact of VTP on lateral coefficient due to dissymmetrical spoiler deployment is analysed in this section

The fig. 27 plots the rolling moment of the configuration with and without tails. One can see that the agreement between numerical calculation with tail and experiment is better than without tail, meaning that interaction between spoiler and tail plays a part.

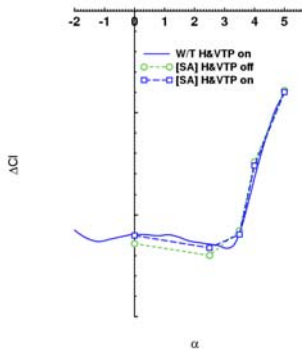

fig. 27 : : Rolling moment, δsp=20° (left wing), M=0.85

An adequate post-processing component allows identifying the contribution of each device and highlights that this additional rolling moment is mainly due to VTP. Indeed, spoiler downwash is seen in almost the same way by both right and left HTP (confirmed by load span distribution on fig 29), thus complete HTP does not create rolling moment. But, the creation of sideslip field of about 1° (see fig. 28) in front of the fin induces a dissymmetry on pressure distribution (see fig 30) and thus a rolling moment

	a/c	wing	Left HTP	Right HTP	VTP
Cl	100 %	105 %	3.4%	- 3.5%	-5%

table 2 : Rolling moment decomposition for each a/c device

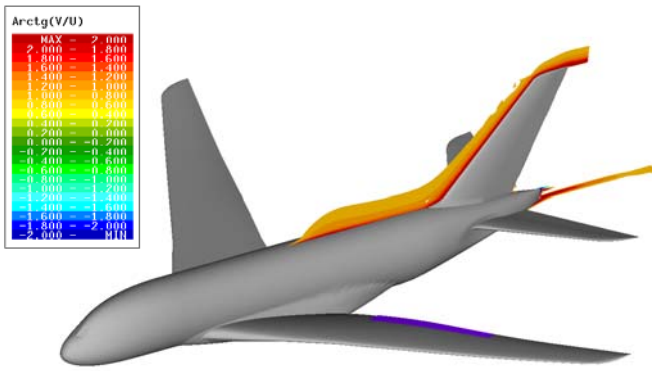

fig. 28 : β field visualization in front of VTP, δs=20° α=2.5°, M=0.85,

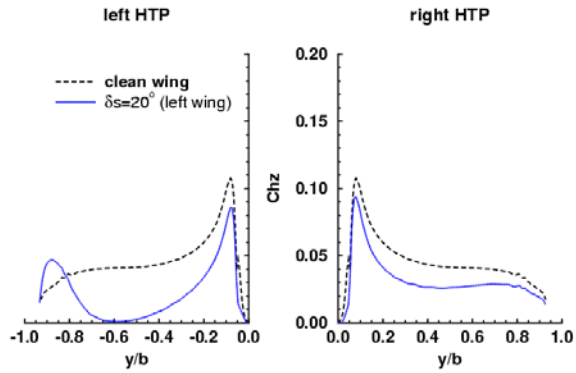

fig 29 : load distribution on left and right HTP, M=0.85, α=2.5°

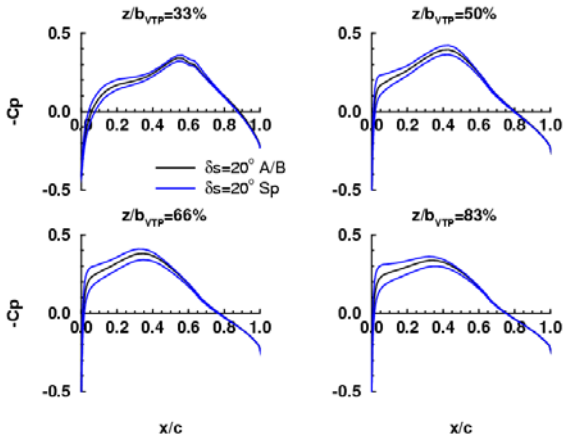

fig 30: Pressure distribution on VTP, M=0.85, α=2.5°

CONCLUSIONS

CFD ability to simulate spoiler and aileron setting has been evaluated throughout comparisons to a dedicated w/t tests campaign on an extruded 2D airfoil equipped with both control devices. Computations involved not only the airfoil but also the w/t upper, lower and lateral walls.

Numerical results of aileron setting are not in close agreement with wind tunnel results, mainly due to a too aft shock position. But in terms of aileron effectiveness, numerical and experimental results are in good agreement. Deployed spoiler configurations have been analyzed by both steady and unsteady numerical approaches. Steady simulations compare fairly to w/t tests on local pressure distributions as well as on global coefficients. Unsteady approach allows simulating the good phenomenon frequency, but the prediction of the average state requires improvement.

The second part of this paper is dedicated to industrial CFD applications in Airbus. Simulations of spoilers and tails were analyzed and compared to experimental results. An interaction between spoiler and horizontal tail plane is demonstrated: HTP induces an effect on spoiler pitching moment effectiveness due to spoiler wake and downwash. Effect of tails on rolling moment due to spoiler is also analyzed, with the conclusion that the major effect is due to VTP.

ACKNOWLEDGMENTS

The experimental and numerical results obtained within the French research project DTP modeling, supported by the French government agencies DGAC and SPAé

REFERENCES

[1] Archambaud, J.P., Mignosi, A., “Two dimensional and Three dimensional adaptation at the T2 transonic wind tunnel of ONERA/CERT”, AIAA paper, May 1998

[2] Archambeau, J.P., Dor, J.B., Michonneau, J.F., Breil J.F., « étude des effets latéraux autour d’un profil bidimensionnel dans la soufflerie T2. Mesure par vélocimétrie laser et utilisation de différents contrôles actifs », PV OA n°15/2891 AN 169D (DERAT n°15/5015.24), octobre 1991

[3] Ayoub, A., Bodapati, S., “Unsteady Flow Patterns Associated with Spoiler Control Device”, AIAA Paper 0127, 1982

[4] Bézard, H., « Calculs Navier-Stokes tri-dimensionnels autour du profil OAT15A dans la soufflerie T2, validation de modèle de turbulence », Rapport technique n° 2/5200.35 DMAE, février 2000

[5] Fillola G., Montagnac, M., Le Pape MC, “Numerical simulation around wing control surfaces”, ICAS 2002, Yokohama

[6] Garbaruk, A., Shur, M., Strelets, M., Spalart, P., “Numerical Study of wind-Tunnel Walls Effects on Transonic Airfoil Flow”, *AIAA journal,* vol.41, n°6, June 2003

[7] Jeanfaivre, G., Benoit, Ch., Le Pape, M.-C. “Improvement of the robustness of the chimera method”, AIAA paper, 02-3290, St Louis, June 2002

[8] Jiang, F., “Assessing Computational Fluid Dynamics Predictions for Control Surface Effectivness”, *Journal of Aircraft*, vol. 38, n°6, 2001

[9] M.Gazaix, A. Jolles, M. Lazareff, “the elsA Object-Oriented Computation tool for industrials applications”, ICAS 2002, Toronto

[10] McLachlan, B.G., Karamcheti, K., Ayoub, A., Seettharam, H.C., “A Study of the Unsteady Flow Field of an Airfoil With Deflected Spoiler”, AIAA Paper 2131, 1983

[11] Steger, J.L., Dougherty, F.C., and Benek, J.A., “A Chimera Grid Scheme”, in Advance in Grid Generation, K.N. Ghia and U. Ghia, eds, ASME FED, Vol. 5 pp. 59-69, 1983